

Multi-Modal Learning with Bayesian-Oriented Gradient Calibration

Peizheng Guo^{1,2}, Jingyao Wang^{1,2}, Huijie Guo^{1,2}, Jiangmeng Li^{1,2},
Chuxiong Sun^{1,2}, Changwen Zheng^{1,2}, Wenwen Qiang^{1,2}

¹University of Chinese Academy of Sciences, ²Institute of Software Chinese Academy of Sciences

Abstract

Multi-Modal Learning (MML) integrates information from diverse modalities to improve predictive accuracy. However, existing methods mainly aggregate gradients with fixed weights and treat all dimensions equally, overlooking the intrinsic gradient uncertainty of each modality. This may lead to (i) excessive updates in sensitive dimensions, degrading performance, and (ii) insufficient updates in less sensitive dimensions, hindering learning. To address this issue, we propose BOGC-MML, a Bayesian-Oriented Gradient Calibration method for MML to explicitly model the gradient uncertainty and guide the model optimization towards the optimal direction. Specifically, we first model each modality’s gradient as a random variable and derive its probability distribution, capturing the full uncertainty in the gradient space. Then, we propose an effective method that converts the precision (inverse variance) of each gradient distribution into a scalar evidence. This evidence quantifies the confidence of each modality in every gradient dimension. Using these evidences, we explicitly quantify per-dimension uncertainties and fuse them via a reduced Dempster-Shafer rule. The resulting uncertainty-weighted aggregation produces a calibrated update direction that balances sensitivity and conservatism across dimensions. Extensive experiments on multiple benchmark datasets demonstrate the effectiveness and advantages of the proposed method.

1 Introduction

Humans perceive the world through multiple sensory modalities, e.g., vision, hearing, and touch. This multi-sensory perception inspires the development of Multi-Modal Learning (MML), which aims to learn a model by integrating information from different modalities to achieve great performance [22, 48]. MML techniques have been successfully applied across various fields, e.g., healthcare [34, 56], autonomous systems [2, 18], human-computer interaction [16, 27], and sentiment analysis [40, 41]. To achieve effective fusion, existing MML approaches mainly rely on gradient-based strategies to combine modality-specific information during the optimization process [5, 37].

Despite existing methods have demonstrated great performance, they still face challenges in determining the optimal direction for optimization. In MML, the gradient of each modality is typically a high-dimensional vector, where each dimension corresponds to the partial derivative of the loss with respect to a specific model parameter [19]. It indicates how a small change in that parameter would affect the model’s output or prediction. Since different modalities exhibit distinct structural patterns and statistical properties, the optimization requirements across the dimensions of these gradients may differ significantly [37]. Take visual-language classification task as an example, the visual modality may be more sensitive to spatial features (e.g., edges or positions), while the language modality may focus more on semantic features (e.g., entity types or sentiment). However, existing methods often aggregate modality gradients using fixed weights and treat all dimensions equally [44, 49, 52]. This overlook of the inherent uncertainty and dimensional sensitivity of modality gradients may lead to

two potential issues: (i) introducing excessive perturbations in sensitive dimensions, which could degrade task performance, and (ii) being overly conservative in relaxed dimensions, may hinder optimization efficiency. **To address these issues, it is crucial to model the uncertainty of each modality in specific gradient dimensions. This help the model to identify which modalities are more reliable and which are less certain in each dimension, leading to more effective updates.**

To this end, we propose a Bayesian-Oriented Gradient Calibration method for MML (BOGC-MML), which explicitly models the uncertainty of modality gradients to achieve more effective optimization in MML. It leverages the concept of confidence [24] as a key measure to quantify the reliability of each modality within each gradient dimension. Instead of treating the gradients as deterministic values, we model them as random variables represented by probability distributions. By quantifying the confidence associated with each modality, we can determine the optimal update direction based on the distribution of these gradients. Specifically, inspired by Bayesian inference [8, 14], we first model the modality gradients as probability distributions (Figure 1). Then, we propose an effective mapping function to convert the precision of each gradient distribution into corresponding evidence (Theorem 4.1). This evidence reflects the confidence of each modality to specific gradient dimension. After obtaining these evidences, we quantify the uncertainties of the modality gradients and adopt the reduced Dempster’s combination rule [20] to aggregate them to determine the optimal update direction. Extensive experiments demonstrate the advantages of the proposed method.

The main contributions can be summarized as follows: (i) We propose BOGC-MML, a novel Bayesian-oriented gradient calibration method for MML. It explicitly models the uncertainty of modality gradients and incorporates the dimensional differences between modality gradients during optimization, making the model update towards the optimal direction. (ii) We present an effective method for estimating evidence from probability distributions with theoretical guarantees. It maps the precision of a probability distribution to its corresponding evidence, enabling more effective gradient aggregation. (iii) Extensive experiments across various benchmarks demonstrate the effectiveness and validity of our proposed method, showcasing its advantages in practice.

2 Related Work

Multi-Modal Learning (MML) seeks to learn an effective model with great performance by integrating information from diverse modalities, such as images, text, and audio [5, 37]. To fuse information across modalities, one effective approach in MML is to focus on gradient optimization. They aggregate gradients across different modalities, as gradient-based optimization plays a crucial role in the model training process. These methods dynamically adjust the contribution of each modality to the gradient aggregation, depending on the context, to enhance the overall performance of the model [39, 46, 49, 51]. For example, [39] adaptively scales each modality’s gradient according to its contribution and adds dynamic Gaussian noise to prevent overfitting; [17] employs a prototypical cross-entropy loss along with early-stage entropy regularization to stimulate slow-learning modalities while preventing dominant ones from overpowering the joint training; [52] analyzes and resolves gradient conflicts between multi-modal and unimodal losses by integrating their directions via Pareto optimization. However, these methods integrate modality gradients with fixed coefficients and assume uniform importance across all modalities, thereby struggling to account for the uncertainty and dimensional sensitivity of these modality gradients. To address these issues, we propose an effective method that quantifies the uncertainty of modality gradients to determine the optimal update direction, thus calibrating optimization. More comparison and discussion are provided in Appendix C.

3 Preliminary

In this section, we introduce the problem settings and fundamental theories related to this work, including MML, Subjective Logic and Evidence Theory, and Dempster-Shafer Evidence Theory.

Multi-Modal Learning (MML). In MML, the goal is to make accurate predictions by effectively integrating information from multiple modalities. To achieve this goal, it is common to jointly optimize via multi-modal fusion loss and unimodal losses [51] (Figure 1). The multi-modal fusion loss is computed based on the combined representation of all modalities and directly guides the model’s predictions. Meanwhile, each unimodal loss supervises the learning of each modality’s representation, encouraging the model to extract important features from each modality.

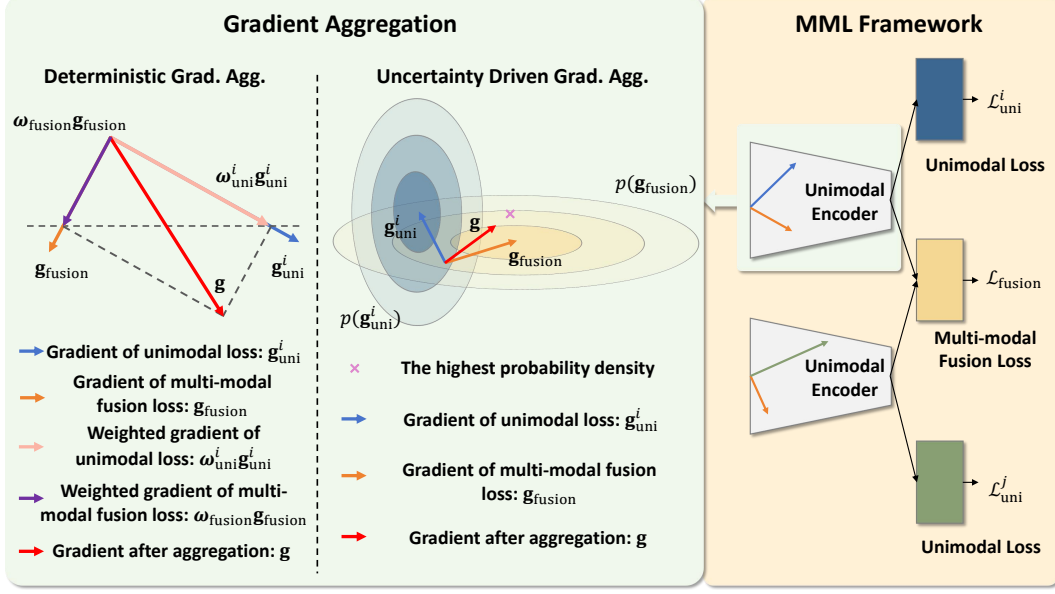


Figure 1: Illustration of MML framework and two kinds of gradient aggregation strategies.

Given a dataset $D^i = \{(x_t^i, y_t)\}_{t=1}^n$ where x_t^i represents the input of the i -th modality for the t -th sample, and y_t is the corresponding ground truth label. The overall loss function is defined as:

$$\mathcal{L}_{\text{total}} = \mathcal{L}_{\text{fusion}} + \varphi \sum_{i=1}^M \mathcal{L}_{\text{uni}}^i, \quad (1)$$

where $\mathcal{L}_{\text{fusion}}$ is the multi-modal fusion loss, $\mathcal{L}_{\text{uni}}^i$ is the unimodal loss for the i -th modality, φ is a regularization parameter, and M is the total number of modalities.

Subjective Logic and Evidence Theory. Subjective logic [24] and evidence theory [6, 45] offer a theoretical framework for directly modeling uncertainty using the Dirichlet distribution (Appendix C.1.2). Specifically, in the context of multi-modal K -class classification, for the i -th modality, the Dirichlet distribution $\text{Dir}(\mu^i | \alpha^i)$ is used, where the parameters $\alpha^i = [\alpha_1^i, \dots, \alpha_K^i]$ are associated with several key concepts from subjective logic and evidence theory, including the evidence $e^i = [e_1^i, \dots, e_K^i]$, belief $b^i = [b_1^i, \dots, b_K^i]$, and uncertainty u^i . The evidence refers to the metrics derived from the input that can support classification [20]. The relationship between the evidence e_k^i and the Dirichlet parameter α_k^i is given by:

$$b_k^i = \frac{e_k^i}{S^i} = \frac{\alpha_k^i - 1}{S^i}, \quad u^i = \frac{K}{S^i}, \quad u^i + \sum_{k=1}^K b_k^i = 1, \quad (2)$$

where $u^i \geq 0$ is the overall uncertainty for the i -th modality, $b_k^i \geq 0$ is the belief mass of k -th class, $S^i = \sum_{k=1}^K \alpha_k^i = \sum_{k=1}^K (e_k^i + 1)$ is known as the Dirichlet strength. From Eq. 2, we can deduce that the more evidence e_k^i is acquired for the k -th class, the higher the belief b_k^i assigned to that class. Conversely, when less evidence e^i is obtained, the uncertainty u^i increases. Building on the concepts of subjective logic and evidence theory [6, 24, 45], in this work, we model the uncertainty of modality gradients to calibrate optimization towards the optimal direction, ensuring that the gradient updates are guided by the reliability of the evidence for each modality.

Dempster-Shafer Evidence Theory (DST). provides a mathematical framework for modeling and integrating uncertain or imprecise information [15]. A fundamental component of DST is Dempster's combination rule, which allows for the fusion of evidence from multiple independent sources. To address the computational challenges of this operation, the Reduced Dempster's combination rule was introduced as an efficient approximation method [20]. In the context of multi-modal K -class classification, given the i -th and j -th modalities, we construct two independent sets, i.e., $\mathbb{M}^i = \{\{b_k^i\}_{k=1}^K, u^i\}$ and $\mathbb{M}^j = \{\{b_k^j\}_{k=1}^K, u^j\}$, which are based on the beliefs and uncertainties of the i -th and j -th modalities, respectively. The combined set \mathbb{M} is obtained by applying the

combination rule $\mathbb{M} = \mathbb{M}^i \oplus \mathbb{M}^j$. The combination rule is defined as:

$$b_k = \frac{b_k^i b_k^j + b_k^i u^j + b_k^j u^i}{1 - C}, \quad u = \frac{u^i u^j}{1 - C} \quad (3)$$

where $C = \sum_{p \neq q} b_p^i b_q^j$ is a measure of the amount of conflict between the two mass sets, $\frac{1}{1-C}$ is a scale factor for normalization. This combination process can be extended to incorporate more than two modalities. Assume we have M modalities, the belief and gradient uncertainty for each modality can be combined iteratively using $\mathbb{M} = \mathbb{M}^1 \oplus \mathbb{M}^2 \dots \oplus \mathbb{M}^M$. In this work, we propose a novel method for uncertainty aggregation of different modality gradients, inspired by the reduced Dempster's combination rule, to more effectively guide the optimization process.

4 Methodology

In this work, we propose BOGC-MML, a Bayesian-oriented gradient calibration method for MML. It calibrates the update direction during MML optimization by incorporating the uncertainty of modality gradients. Specifically, we first model the gradient of each modality as a probability distribution using Bayesian inference. We then derive the gradient distribution for the multi-modal fusion loss (Section 4.1). Next, we propose an effective method for estimating evidence from these probability distributions. This is achieved by estimating the evidence via a power mapping that is based on the precision of the probability distributions (Theorem 4.1). Using the estimated evidence, we quantify the uncertainties of the modality-specific gradients and the gradient of the multi-modal fusion loss, drawing from subjective logic and evidence theory. Finally, based on the quantified uncertainties, we perform uncertainty-driven gradient aggregation using the reduced Dempster's combination rule to obtain a more precise update direction, calibrating the MML optimization (Section 4.2).

4.1 Bayesian-based Gradient Probability Distribution

In this subsection, we model the uncertainty of modality gradients by deriving their probability distributions using Bayesian inference [8, 14]. Specifically, we begin by treating the parameters of the last network layer before the output as random variables and estimate their posterior distributions using the Laplace approximation [28] (Subsection 4.1.1). Next, we reformulate the gradient of each modality as a quadratic function of the associated parameters, and then approximate the gradient distribution by calculating the first and second-order moments (Section 4.1.2). Obtaining the gradient distribution of each modality, we derive the gradient of the multi-modal fusion loss and obtain its corresponding probability distribution under the Gaussian priors (Section 4.1.3).

4.1.1 Posterior Estimation of Network Parameters

In MML, network architectures typically consist of modality-specific encoders, modality fusion layers, and classification heads [5, 37]. We consider the parameters Θ of the last layer before output as random variables and compute their probability distributions. Assuming that the posterior distribution of the parameters is a Gaussian distribution, which is a mild assumption [36], we approximate the posterior using the Laplace approximation [28]. Formally, given the observed data \mathcal{D} , the posterior distribution can be formulated according to Bayesian rule:

$$p(\Theta \mid \mathcal{D}) \propto p(\mathcal{D} \mid \Theta) \cdot p(\Theta). \quad (4)$$

Then, we approximate the posterior distribution of the parameters via a second-order Taylor expansion and Laplace approximation: for the i -th modality, the posterior distribution of the parameters Θ^i is:

$$\log p(\Theta^i \mid \mathcal{D}) \approx \log p(\hat{\Theta}^i \mid \mathcal{D}) + (-\nabla_{\Theta^i} \log p(\mathcal{D}, \Theta^i))^\top \Delta \Theta^i + \frac{1}{2} (\Delta \Theta^i)^\top \mathbf{H}^i \Delta \Theta^i, \quad (5)$$

where $\hat{\Theta}^i$ is the learned point estimate of the parameters, $\Delta \Theta^i = \Theta^i - \hat{\Theta}^i$ is the deviation from the estimate, and $\mathbf{H}^i = -\nabla_{\Theta^i}^2 \log p(\mathcal{D}, \Theta^i)$ is the negative Hessian matrix of the joint log-likelihood with respect to $p(\mathcal{D}, \Theta^i)$. Then, we omit the first-order term (i.e. $(-\nabla_{\Theta^i} \log p(\mathcal{D}, \Theta^i))^\top \Delta \Theta^i$) in the Taylor expansion. As a result, the posterior takes the quadratic form: $\log p(\Theta^i \mid \mathcal{D}) \approx c^i + \frac{1}{2} (\Delta \Theta^i)^\top \mathbf{H}^i \Delta \Theta^i$, where c^i absorbs terms independent of Θ^i . The corresponding Gaussian distribution is (The detailed derivations can be found in Appendix C.3):

$$p(\Theta^i \mid \mathcal{D}) \approx \mathcal{N}(\Theta^i \mid (\hat{\Theta}^i - (\mathbf{H}^i)^{-1} \mathbf{q}^i), (\mathbf{H}^i)^{-1}). \quad (6)$$

However, the Hessian \mathbf{H}^i is often not positive-definite [1, 12, 13]. Thus, we replace it with the generalized Gauss-Newton matrix, which provides a more stable approximation for optimization:

$$\tilde{\mathbf{H}}^i = \sum_{j=1}^{|\mathcal{D}_{batch}|} (\mathbf{J}_j^i)^\top \mathbf{B}_j^i \mathbf{J}_j^i + (\mathbf{V}_p^i)^{-1}, \quad (7)$$

where $|\mathcal{D}_{batch}|$ is the batch size, $\mathbf{J}_j^i = \nabla_{\Theta^i} \mathbf{f}^i(X_j; \Theta^i)$ is the Jacobian of the model output for the i -th modality with respect to its parameters, $\mathbf{B}_j^i = \nabla_{\mathbf{f}^i}^2(-\log p(Y_j^i | X_j, \Theta^i))$ is the Hessian of the negative log-likelihood with respect to the model outputs, and \mathbf{V}_p^i is the covariance of the Gaussian prior for Θ^i . Thus, the posterior approximation is:

$$p(\Theta^i | \mathcal{D}) \approx \mathcal{N}(\Theta^i | (\hat{\Theta}^i - (\mathbf{H}^i)^{-1} \mathbf{q}^i), \tilde{\mathbf{H}}^i). \quad (8)$$

4.1.2 Gradient Distribution of Single Modality

Based on the obtained posterior distributions, in this subsection, we aim to approximate the gradient probability distribution of the modalities. Specifically, we first establish the functional dependence of the gradient on the parameters. Then, we compute the first and second-order moments of the gradient through Monte Carlo sampling [43]. Finally, the gradient distribution is approximated by a Gaussian distribution, from which the corresponding mean and covariance are derived.

Given the i -th modality and a random batch of samples $\mathcal{D}_{batch} \sim \mathcal{D}$, the gradient of the square loss with respect to the shared hidden layer ψ for the t -th sample is derived as follows:

$$\mathbf{g}_t^i = \frac{\partial \mathcal{L}_t^i}{\partial \hat{Y}_t^i} \frac{\partial \hat{Y}_t^i}{\partial \psi_t} = 2\Theta^i \psi_t^\top \Theta^i - 2\Theta^i Y_t^i, \quad (9)$$

where $\mathcal{L}_t^i = (Y^i - \hat{Y}^i)^2$ is the square loss between label Y^i and network output \hat{Y}^i for modality i .

Eq. 9 defines the functional relationship between the gradient and the model parameters. Specifically, \mathbf{g}_t^i is a quadratic function of the random variable Θ^i , which follows a Gaussian distribution. Consequently, \mathbf{g}_t^i is also a random variable, and it follows a generalized chi-square distribution. Since this distribution lacks a closed-form density function, we approximate \mathbf{g}_t^i using a Gaussian distribution [42]. We optimize the parameters of the Gaussian approximation by matching the first and second-order moment to maximize its similarity to the true distribution [33].

In classification tasks, the gradient exhibits a nonlinear dependency on the model parameters, which precludes a closed-form solution for the first and second order moments [7, 54]. To solve this issue, we adopt Monte Carlo sampling [43] for approximation. Monte Carlo sampling only requires drawing samples from the posterior distribution and computing the gradient for each sample, without relying on the specific structure of the model [43, 53]. Thus, given n samples, we can derive the mean and covariance of the Gaussian approximation as follows:

$$\boldsymbol{\mu}_t^i := \mathbb{E}[\mathbf{g}_t^i] \approx \frac{1}{n} \sum_{j=1}^n \mathbf{g}_t^i(\Theta_j^i), \quad \boldsymbol{\Sigma}_t^i := \mathbb{E}[(\mathbf{g}_t^i)^2] - \boldsymbol{\mu}_t^i(\boldsymbol{\mu}_t^i)^\top \approx \frac{1}{n} \sum_{j=1}^n \mathbf{g}_t^i(\Theta_j^i) \mathbf{g}_t^i(\Theta_j^i)^\top - \boldsymbol{\mu}_t^i(\boldsymbol{\mu}_t^i)^\top, \quad (10)$$

where $\boldsymbol{\Lambda}_t^i = \frac{1}{\boldsymbol{\Sigma}_t^i}$ is the precision matrix, $\boldsymbol{\Sigma}_t^i$ and $\boldsymbol{\Lambda}_t^i$ are both K -dimensional matrices, and Θ_j^i are samples from $p(\Theta^i | \mathcal{D}_{batch})$. The probability distribution of \mathbf{g}_t^i can be expressed as:

$$p(\mathbf{g}_t^i) \approx \mathcal{N}(\mathbf{g}_t^i | \boldsymbol{\mu}_t^i, \boldsymbol{\Sigma}_t^i). \quad (11)$$

4.1.3 Gradient Distribution of The Multi-Modal Fusion Loss

Obtaining the gradient distribution of each modality, in this subsection, we aim to obtain the probability distribution for the gradient of the multi-modal fusion loss \mathcal{L}_{fusion} . We proceed in two steps: (i) first derive the expression of the gradient of \mathcal{L}_{fusion} , and (ii) then calculate the probability distribution for the gradient of \mathcal{L}_{fusion} based on the Gaussian priors [38].

For the first step, in MML, the fusion loss \mathcal{L}_{fusion} can be expressed as $\mathcal{L}_{fusion} = \mathcal{L}(\mathcal{C}(\zeta^1 \oplus \zeta^2 \oplus \dots \oplus \zeta^m), y)$, where ζ^i is a deep network with parameters θ^i used to process the i -th modality, \mathcal{C} is a

classifier, and \oplus denotes a fusion operation (e.g., concatenation). Given the t -th sample, we obtain the the gradient of $\mathcal{L}_{\text{fusion}}$, i.e. $\mathbf{g}_t^{\text{fusion}} = \frac{1}{M} \sum_{i=1}^M \mathbf{g}_t^i$. Furthermore, since the Gaussian distribution remains Gaussian after weighted sum [38], we can obtain the mean and covariance of $\mathbf{g}_t^{\text{fusion}}$ based on the gradient probability distributions of each modality, which can be expressed as:

$$\boldsymbol{\mu}_t^{\text{fusion}} = \frac{1}{M} \sum_{i=1}^M \boldsymbol{\mu}_t^i, \quad \boldsymbol{\Sigma}_t^{\text{fusion}} = \frac{1}{M} \sum_{i=1}^M \boldsymbol{\Sigma}_t^i, \quad (12)$$

where $\boldsymbol{\Sigma}_t^{\text{fusion}}$ is also a K -dimensional matrix. Thus, the probability distribution of $\mathbf{g}_t^{\text{fusion}}$ is:

$$p(\mathbf{g}_t^{\text{fusion}}) \approx \mathcal{N}(\mathbf{g}_t^{\text{fusion}} | \boldsymbol{\mu}_t^{\text{fusion}}, \boldsymbol{\Sigma}_t^{\text{fusion}}). \quad (13)$$

In summary, in this subsection, we first capture the uncertainty of each modality by modeling its gradient distribution through the posterior distribution. This approach yields a richer, probabilistic description of the individual gradient spaces. Building on these per-modality distributions, we then derive the Gaussian distribution for the fused gradient $\mathbf{g}_t^{\text{fusion}}$ of the multi-modal fusion loss $\mathcal{L}_{\text{fusion}}$.

4.2 Uncertainty Driven Gradient Aggregation

Based on the above results, in this subsection, we aggregate the gradient of each modality \mathbf{g}_t^i with the gradient $\mathbf{g}_t^{\text{fusion}}$ of the multi-modal loss under the uncertainty modeling framework, and use the aggregated results to get the optimal gradient update direction. Specifically, inspired by subjective logic [24] and evidence theory [6, 45], we propose an effective method to convert each gradient into Dirichlet concentration parameters and associated evidence values. From these, we compute the belief masses and uncertainty for each gradient in every dimension. Next, we fuse these beliefs and uncertainties across the gradients using the reduced Dempster's combination rule, yielding a joint belief and a joint uncertainty per dimension. Finally, we weight and sum \mathbf{g}_t^i and $\mathbf{g}_t^{\text{fusion}}$ according to the fused belief and uncertainty, producing the calibrated update direction for the i -th modality.

Given the i -th modality and t -th sample, the covariance matrix $\boldsymbol{\Sigma}_t^i$ and the precision matrix $\boldsymbol{\Lambda}_t^i$ are both K -dimension (Eq.10). The element of the d -th row and d -th column in $\boldsymbol{\Lambda}_t^i$ is the precision of \mathbf{g}_t^i in the d -th dimension. Similarly, the precision of $\mathbf{g}_t^{\text{fusion}}$ in the d -th dimension can be obtained according to Eq.13, i.e., $\lambda_{t,d}^i = (\boldsymbol{\Sigma}_t^i)^{-1}[d, d]$ and $\lambda_{t,d}^{\text{fusion}} = (\boldsymbol{\Sigma}_t^{\text{fusion}})^{-1}[d, d]$. Then, we propose:

Theorem 4.1 *Given a Gaussian distribution $\theta \sim \mathcal{N}(\mu_0, \frac{1}{\lambda_0})$. Given n observations x_1, \dots, x_n and the observation noise precision (inverse variance) is $\tau > 0$, the likelihood is $p(x_{1:n} | \theta) = \prod_{i=1}^n \mathcal{N}(x_i | \theta, \frac{1}{\tau})$. Given a real number exponent $s > 0$ and a mapping $\phi: (0, \infty) \rightarrow (0, \infty)$ where $\phi(\lambda) = \lambda^s$, its scalar evidence can be estimated as $e = \phi(\lambda_n) = (\lambda_0 + n\tau)^s$.*

Theorem 4.1 provides a method to convert the parameter posterior precision, which is obtained by combining a Gaussian prior with observed data, into a single evidence value via a continuous monotonic mapping. First, the prior and data merge into a posterior precision (inverse variance), and then an exponent-controlled mapping translates that precision into evidence. The resulting evidence both captures the amount of information and allows us to adjust how sensitively it responds to changes in precision, unifying prior knowledge and observed uncertainty into one coherent measure.

According to Theorem 4.1, for the d -th dimension, we construct a power mapping $\phi(\cdot)$ to calculate the evidence $e_{t,d}^i$ of \mathbf{g}_t^i . Then, we compute Dirichlet concentration parameter $\alpha_{t,d}^i$ of \mathbf{g}_t^i . In the same way, we can obtain the evidence $e_{t,d}^{\text{fusion}}$ and Dirichlet concentration parameter $\alpha_{t,d}^{\text{fusion}}$ of $\mathbf{g}_t^{\text{fusion}}$.

$$\begin{aligned} e_{t,d}^i &= \phi(\lambda_{t,d}^i) = (\lambda_{t,d}^i)^s, \quad \alpha_{t,d}^i = e_{t,d}^i + 1, \\ e_{t,d}^{\text{fusion}} &= \phi(\lambda_{t,d}^{\text{fusion}}) = (\lambda_{t,d}^{\text{fusion}})^s, \quad \alpha_{t,d}^{\text{fusion}} = e_{t,d}^{\text{fusion}} + 1. \end{aligned} \quad (14)$$

Then, according to subjective logic [24] and evidence theory [6, 45], we compute the belief masses (i.e. $b_{t,d}^i$ and $b_{t,d}^{\text{fusion}}$) and uncertainties (i.e. u_t^i and u_t^{fusion}) of \mathbf{g}_t^i and $\mathbf{g}_t^{\text{fusion}}$ respectively.

$$\begin{aligned} S_t^i &= \sum_{d=1}^K \alpha_{t,d}^i, \quad b_{t,d}^i = \frac{e_{t,d}^i}{S_t^i}, \quad u_t^i = \frac{K}{S_t^i}, \\ S_t^{\text{fusion}} &= \sum_{d=1}^K \alpha_{t,d}^{\text{fusion}}, \quad b_{t,d}^{\text{fusion}} = \frac{e_{t,d}^{\text{fusion}}}{S_t^{\text{fusion}}}, \quad u_t^{\text{fusion}} = \frac{K}{S_t^{\text{fusion}}}, \end{aligned} \quad (15)$$

where S_t^i and S_t^{fusion} are known as Dirichlet strength. After that, we construct sets of mass $\mathbb{M}_t^i = \{\{b_{t,d}^i\}_{d=1}^K, u_t^i\}$ and $\mathbb{M}_t^{\text{fusion}} = \{\{b_{t,d}^{\text{fusion}}\}_{d=1}^K, u_t^{\text{fusion}}\}$ with the Dempster-Shafer rules, and combine them to obtain a joint mass $\mathbb{M} = \{b_{t,d}, u_t\}$ according to Eq.3:

$$b_{t,d} = \frac{b_{t,d}^i b_{t,d}^{\text{fusion}} + b_{t,d}^i u_t^{\text{fusion}} + b_{t,d}^{\text{fusion}} u_t^i}{1 - C}, \quad u_t = \frac{u_t^i u_t^{\text{fusion}}}{1 - C} \quad (16)$$

where $C = \sum_{p \neq q} b_{tp}^i b_{tq}^{\text{fusion}}$ is a measure of the amount of conflict between the two mass sets. Then, we can obtain the gradient \mathbf{g}_{DS} after aggregation as follows:

$$\mathbf{g}_{\text{DS}} = \sum_{t=1}^n \sum_{d=1}^K b_{t,d} (b_{t,d}^i \boldsymbol{\mu}_{t,d}^i + b_{t,d}^{\text{fusion}} \boldsymbol{\mu}_{t,d}^{\text{fusion}}), \quad (17)$$

where $\boldsymbol{\mu}_{t,d}^i$ and $\boldsymbol{\mu}_{t,d}^{\text{fusion}}$ are the values of $\boldsymbol{\mu}_t^i$ and $\boldsymbol{\mu}_t^{\text{fusion}}$ in the d -th dimension, respectively.

To this end, we can obtain a more effective and efficient gradient optimization direction considering the gradient uncertainty across modalities. Briefly, our method first captures the full uncertainty of each modality by modeling its gradient as a probability distribution, yielding a richer representation of the gradient space. We then convert each gradient distribution’s precision into a scalar evidence measure, which in turn allows us to quantify the uncertainty of every modality gradient. Finally, we fuse these per-modality uncertainties using a reduced Dempster-Shafer rule to calibrate the combined update direction, thereby guiding more reliable and balanced optimization in MML.

5 Experiment

In this section, we conduct extensive experiments on various benchmark datasets to verify the effectiveness of BOGC-MML. More details and experiments are provided in **Appendices D-G**.

5.1 Experimental Settings

Datasets We conduct experiments on three representative benchmark datasets: (i) **CREMA-D** [9] is an audio-visual dataset encompassing 7,442 video clips that depict 6 common emotional expressions (e.g., happiness, sadness, anger), performed by 91 professional actors; (ii) **Kinetics Sounds** [3] is a large-scale audio-visual dataset comprising approximately 19,000 video clips across 31 human action categories (e.g., clapping, drumming, jumping), designed to support research in cross-modal action recognition; (iii) **BraTS** [31] is a multimodal medical imaging dataset with 285 training and 66 validation samples, each providing four MRI modalities (Flair, T1, T1c, T2), and serves as a standard benchmark for brain tumor segmentation, particularly under scenarios involving missing modalities.

Implementation Details Unless otherwise specified, all experiments are conducted using a ResNet-18 backbone as the default architecture configuration, with models trained from scratch without any pre-trained weights. We learn the posterior distribution over the parameters of the final layer in each modality-specific encoder. For optimization, we use stochastic gradient descent (SGD) with a momentum of 0.9 and a scaling factor $\gamma = 1.5$. The initial learning rate is set to 0.1 and can be linearly scaled if necessary. All results are averaged over five runs on NVIDIA Tesla V100 GPUs.

5.2 Performance Comparison

In this subsection, we evaluate the effectiveness of the proposed BOGC-MML method. Following the same experimental settings in MMPareto [52], we conduct comparative studies on the CREMA-D and Kinetics Sounds datasets. We compare our method with several representative multimodal methods, including G-Blending [51], OGM-GE [39], Greedy [55], PMR [17], AGM [26], TMC [20], ECML [57], and MMPareto [52]. In addition, we adopt several different training setups: **Audio and Video-only** are unimodal models and trained independently; **Unimodal pre-trained & fine-tune** refers to fine-tuning a multimodal model initialized with separately pre-trained unimodal encoders; **One joint loss** uses only the multimodal joint loss for optimization. **Uniform baseline** computes the final loss by equally summing multimodal and unimodal losses. Note that to support comprehensive comparison, we also conduct experiments across traditional CNN and Transformer-based architectures.

Table 1: Classification accuracy(%) on CREMA-D and Kinetics Sounds. The best results are shown in **bold**. * indicates that the unimodal accuracy (Acc audio and Acc video) is obtained by fine-tuning a unimodal classifier with the trained unimodal encoder frozen.

Method	CREMA-D				Kinetics Sounds			
	Acc	Acc audio	Acc video	Worst Acc	Acc	Acc audio	Acc video	Worst Acc
Audio-only	-	61.69	-	-	-	53.63	-	-
Video-only	-	-	56.05	-	-	-	49.20	-
Unimodal pre-trained & fine-tune	71.51	60.08	60.22	68.51	68.75	53.49	50.07	66.75
One joint loss*	66.13	59.27	36.56	63.63	64.61	52.03	35.47	61.61
Uniform baseline	71.10	63.44	51.34	69.30	68.31	53.20	40.55	66.11
G-Blending [51]	72.01	60.62	52.23	69.31	68.90	52.11	41.35	65.40
OGM [39]*	69.19	56.99	40.05	66.89	66.79	51.09	37.86	64.90
Greedy [55]*	67.61	60.69	38.17	65.51	65.32	50.58	35.97	62.52
PMR [17]*	66.32	59.95	32.53	64.62	65.70	52.47	34.52	62.30
AGM [26]*	70.06	60.38	37.54	68.06	66.17	51.31	34.83	63.67
TMC [20]	72.84	61.73	52.25	69.76	70.17	55.53	50.83	67.64
ECML [57]	74.68	62.31	53.16	71.77	71.25	56.24	51.35	68.08
MMPareto [52]	75.13	65.46	55.24	71.93	70.13	56.40	53.05	67.33
Ours	78.91	68.52	58.79	74.02	72.64	58.11	56.89	69.37

Table 2: Test performance on CREMA-D and Kinetics Sounds where **bold** and underline represent the best and runner-up respectively. The network follows transformer-based framework MBT [35].

Method	CREMA-D				Kinetics Sounds			
	from scratch		with pretrain		from scratch		with pretrain	
	Acc	macro F1	Acc	macro F1	Acc	macro F1	Acc	macro F1
One joint loss	44.96	42.78	66.69	67.26	42.51	41.56	68.30	69.31
Uniform baseline	45.30	43.74	69.89	70.11	43.31	43.08	69.40	69.60
G-Blending [51]	46.38	45.16	69.91	70.01	44.69	44.19	69.41	69.47
OGM-GE [39]	42.88	39.34	65.73	65.88	41.79	41.09	69.55	69.53
Greedy [55]	44.49	42.76	66.67	67.26	43.31	43.08	69.62	69.75
PMR [17]	44.76	42.95	65.59	66.07	43.75	43.21	69.67	69.87
AGM [26]	45.36	43.81	66.54	67.75	43.65	43.57	69.59	69.14
TMC [20]	46.83	46.26	68.96	69.61	43.91	43.95	69.02	68.56
ECML [57]	48.00	47.26	70.11	70.86	45.13	44.75	70.12	69.61
MMPareto [52]	48.66	48.17	70.43	71.17	45.20	45.26	70.28	70.11
Ours	52.21	50.06	74.00	73.01	47.19	47.36	73.17	74.08

As shown in **Table 1**, our method consistently achieves superior performance, outperforming both unimodal and multimodal baselines. Furthermore, **Table 2** presents a performance comparison on the CREMA-D and Kinetics Sounds datasets using a transformer-based framework MBT [35], evaluated by accuracy (Acc) and macro F1-score under two training setups: training from scratch and pretraining. Our method again achieves the best results, reaching 74.00% accuracy on CREMA-D dataset and 73.17% on Kinetics Sounds dataset (both with pretraining), significantly outperforming baselines. These results further validate the effectiveness and advantages of the proposed BOGC-MML.

5.3 Performance on Missing Modality

To further evaluate the performance of the proposed BOGC-MML method, we conduct comparative experiments under missing modality. Specifically, we assess BOGC-MML against several strong baselines [4, 47, 50] across all 15 possible missing modality combinations on the BraTS dataset.

From the results in **Table 3**, we can observe that (i) BOGC-MML consistently achieves performance that is comparable to or superior to existing SOTA methods, even under various missing modality scenarios. For example, with Flair and T1c, BOGC-MML reaches over 2.8% higher than LCKD and nearly 6.5% above mmFm. In the setting of full-modality availability, BOGC-MML achieves a 3.7% boost over the strongest baseline. (ii) BOGC-MML significantly reduces the accuracy gap across different modalities, particularly narrowing the difference between the more challenging F1 and T1 modalities and the relatively easier T1c modality. For instance, in the Enhancing Tumour subtask with only T1c available, BOGC-MML achieves a relative improvement of 3.2% over the strongest baseline. These results demonstrate the advantage of the proposed BOGC-MML in practice.

Table 3: Top-1 classification accuracy(%) under missing modalities on the BraTS Dataset. • and ◦ denote present and missing modalities, respectively. The best results are in **bold**.

Modalities		Enhancing Tumour					Tumour Core					Whole Tumour				
Fi	T1 T1c T2	HMIS	RSeg	mmFm	LCKD	BOGC-MML	HMIS	RSeg	mmFm	LCKD	BOGC-MML	HMIS	RSeg	mmFm	LCKD	BOGC-MML
• ◦ ◦ ◦		11.78	25.69	39.33	45.48	47.97	26.06	53.57	61.21	72.01	75.56	52.48	85.69	86.10	89.45	92.36
◦ • ◦ ◦		10.16	17.29	32.53	43.22	46.42	37.39	47.90	56.55	66.58	69.21	57.62	70.11	67.52	76.48	78.96
◦ ◦ • ◦		62.02	67.07	72.60	75.65	77.86	65.29	76.83	75.41	83.02	85.94	61.53	73.31	72.22	77.23	79.11
◦ ◦ ◦ •		25.63	28.97	43.05	47.19	49.77	57.20	57.49	64.20	70.17	73.01	80.96	82.24	81.15	84.37	86.95
• • ◦ ◦		10.71	32.13	42.96	48.30	51.21	41.12	60.68	65.91	74.58	77.32	64.62	88.24	87.06	89.97	93.03
• ◦ • ◦		66.10	70.30	75.07	78.75	81.56	71.49	80.62	77.88	85.67	87.42	68.99	88.51	87.30	90.47	92.71
• ◦ ◦ •		30.22	33.84	47.52	49.01	53.11	57.68	61.16	69.75	75.41	78.25	82.95	88.28	87.59	90.39	93.78
◦ • • ◦		66.22	69.06	74.04	76.09	78.98	72.46	78.72	78.59	82.49	86.85	68.47	77.18	74.42	80.10	83.54
◦ • ◦ •		32.39	32.01	44.99	50.09	52.87	60.92	62.19	69.42	72.75	76.02	82.41	84.78	82.20	86.05	88.77
◦ ◦ • •		67.83	69.71	74.51	76.01	79.31	76.64	80.20	78.61	84.85	86.89	82.48	85.19	82.99	86.49	89.72
• • • ◦		68.54	70.78	75.47	77.78	80.41	76.01	81.06	79.80	85.24	88.10	72.31	88.73	87.33	90.50	93.24
• • • •		31.07	36.41	47.70	49.96	51.92	60.32	64.38	71.52	76.68	79.70	83.43	88.81	87.75	90.46	92.82
• ◦ • •		68.72	70.88	75.67	77.48	80.21	77.53	80.72	79.55	85.56	87.76	83.85	89.27	88.14	90.90	93.37
◦ • • •		69.92	70.10	74.75	77.60	79.82	78.96	80.33	80.39	84.02	87.33	83.94	86.01	82.71	86.73	89.11
• • • •		70.24	71.13	77.61	79.33	83.01	79.48	80.86	85.78	85.31	88.61	84.74	89.45	89.64	90.84	93.76

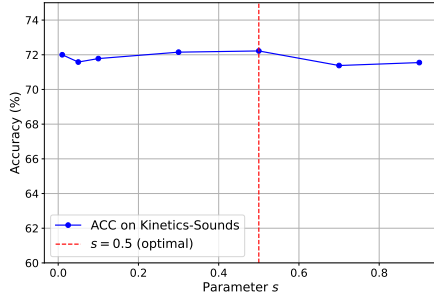


Figure 2: Parameter sensitivity about the parameters s on Kinetics-Sounds dataset.

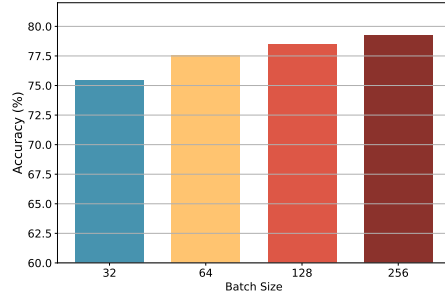


Figure 3: Accuracy comparison on CREMA-D dataset under different batch sizes.

5.4 Ablation Study

We conduct a series of ablation studies to evaluate the best parameterization and implementation choices. More details and results, e.g., the trade-off results, are provided in Appendix G.

Parameter Sensitivity of Hyperparameter s We conduct a parameter sensitivity experiment to evaluate the impact of the parameter s , which is used to compute the evidential value of variables. The values of s are selected from the range $[0.01, 0.05, 0.1, 0.3, 0.5, 0.7, 0.9]$. The experiment is conducted on the Kinetics-Sounds dataset. The experimental results, as shown in Figure 2, indicate that the parameter s has a relatively minor influence on the overall performance.

Ablation Study about Batch Size We investigate the impact of the training batch size. The values are chosen from $[32, 64, 128, 256]$ with grid search. The experiment is conducted on the CREMA-D dataset, and the results are presented in Figure 3. From the results, we can observe that the batch size has little effect on our method, which proves the stability of the proposed method.

6 Conclusion

In this work, we investigate the role of uncertainty in modality-specific gradients for Multi-Modal Learning and introduce a novel calibration strategy that unifies Bayesian inference with evidence theory. First, we leverage Bayesian inference to model the gradient of each modality as a probability distribution over network weights, capturing a richer, uncertainty-aware view of the gradient space. Next, using Dirichlet distributions and subjective logic, we propose an effective way to convert these gradient distributions into evidential measures that directly quantify per-dimension confidence. Finally, drawing on Dempster-Shafer theory, we fuse the modality-specific evidence to compute a consolidated, uncertainty-weighted update direction for MML optimization. Extensive experiments across multiple benchmark datasets demonstrate the advantage of our method.

References

- [1] Idan Achituve, Idit Diamant, Arnon Netzer, Gal Chechik, and Ethan Fetaya. Bayesian uncertainty for gradient aggregation in multi-task learning. In *Proceedings of the 41st International Conference on Machine Learning*, pages 117–134, 2024.
- [2] Bless Lord Y Agbley, Jianping Li, Amin Ul Haq, Edem Kwedzo Bankas, Sultan Ahmad, Isaac Osei Agyemang, Delanyo Kulevome, Waldiodio David Ndiaye, Bernard Cobbinah, and Shoistamo Latipova. Multimodal melanoma detection with federated learning. In *2021 18th international computer conference on wavelet active media technology and information processing (ICCWAMTIP)*, pages 238–244. IEEE, 2021.
- [3] Relja Arandjelovic and Andrew Zisserman. Look, listen and learn. In *Proceedings of the IEEE international conference on computer vision*, pages 609–617, 2017.
- [4] Spyridon Bakas, Mauricio Reyes, Andras Jakab, Stefan Bauer, Markus Rempfler, Alessandro Crimi, Russell Takeshi Shinohara, Christoph Berger, Sung Min Ha, Martin Rozycki, et al. Identifying the best machine learning algorithms for brain tumor segmentation, progression assessment, and overall survival prediction in the brats challenge. *arXiv preprint arXiv:1811.02629*, 2018.
- [5] Tadas Baltrušaitis, Chaitanya Ahuja, and Louis-Philippe Morency. Multimodal machine learning: A survey and taxonomy. *IEEE transactions on pattern analysis and machine intelligence*, 41(2):423–443, 2018.
- [6] Wentao Bao, Qi Yu, and Yu Kong. Evidential deep learning for open set action recognition. In *Proceedings of the IEEE/CVF international conference on computer vision*, pages 13349–13358, 2021.
- [7] Christopher M Bishop and Nasser M Nasrabadi. *Pattern recognition and machine learning*, volume 4. Springer, 2006.
- [8] George EP Box and George C Tiao. *Bayesian inference in statistical analysis*. John Wiley & Sons, 2011.
- [9] Houwei Cao, David G Cooper, Michael K Keutmann, Ruben C Gur, Ani Nenkova, and Ragini Verma. Crema-d: Crowd-sourced emotional multimodal actors dataset. *IEEE transactions on affective computing*, 5(4):377–390, 2014.
- [10] Bertrand Charpentier, Daniel Zügner, and Stephan Günnemann. Posterior network: Uncertainty estimation without ood samples via density-based pseudo-counts. *Advances in neural information processing systems*, 33:1356–1367, 2020.
- [11] Cheng Chen, Qi Dou, Yueming Jin, Hao Chen, Jing Qin, and Pheng-Ann Heng. Robust multimodal brain tumor segmentation via feature disentanglement and gated fusion. In *Medical Image Computing and Computer Assisted Intervention—MICCAI 2019: 22nd International Conference, Shenzhen, China, October 13–17, 2019, Proceedings, Part III 22*, pages 447–456. Springer, 2019.
- [12] Anna Choromanska, Mikael Henaff, Michael Mathieu, Gérard Ben Arous, and Yann LeCun. The loss surfaces of multilayer networks. In *Artificial intelligence and statistics*, pages 192–204. PMLR, 2015.
- [13] Yann N Dauphin, Razvan Pascanu, Caglar Gulcehre, Kyunghyun Cho, Surya Ganguli, and Yoshua Bengio. Identifying and attacking the saddle point problem in high-dimensional non-convex optimization. *Advances in neural information processing systems*, 27, 2014.
- [14] Arthur P Dempster. A generalization of bayesian inference. *Journal of the Royal Statistical Society: Series B (Methodological)*, 30(2):205–232, 1968.
- [15] Arthur P Dempster. Upper and lower probabilities induced by a multivalued mapping. In *Classic works of the Dempster-Shafer theory of belief functions*, pages 57–72. Springer, 2008.
- [16] Sidney K D’mello and Jacqueline Kory. A review and meta-analysis of multimodal affect detection systems. *ACM computing surveys (CSUR)*, 47(3):1–36, 2015.
- [17] Yunfeng Fan, Wenchao Xu, Haozhao Wang, Junxiao Wang, and Song Guo. Pmr: Prototypical modal rebalance for multimodal learning. In *Proceedings of the IEEE/CVF Conference on Computer Vision and Pattern Recognition*, pages 20029–20038, 2023.

- [18] Di Feng, Christian Haase-Schütz, Lars Rosenbaum, Heinz Hertlein, Claudius Glaeser, Fabian Timm, Werner Wiesbeck, and Klaus Dietmayer. Deep multi-modal object detection and semantic segmentation for autonomous driving: Datasets, methods, and challenges. *IEEE Transactions on Intelligent Transportation Systems*, 22(3):1341–1360, 2020.
- [19] Ian Goodfellow, Yoshua Bengio, Aaron Courville, and Yoshua Bengio. *Deep learning*, volume 1. MIT press Cambridge, 2016.
- [20] Zongbo Han, Changqing Zhang, Huazhu Fu, and Joey Tianyi Zhou. Trusted multi-view classification with dynamic evidential fusion. *IEEE transactions on pattern analysis and machine intelligence*, 45(2):2551–2566, 2022.
- [21] Mohammad Havaei, Nicolas Guizard, Nicolas Chapados, and Yoshua Bengio. Hemis: Hetero-modal image segmentation. In *Medical Image Computing and Computer-Assisted Intervention–MICCAI 2016: 19th International Conference, Athens, Greece, October 17–21, 2016, Proceedings, Part II 19*, pages 469–477. Springer, 2016.
- [22] Yu Huang, Chenzhuang Du, Zihui Xue, Xuanyao Chen, Hang Zhao, and Longbo Huang. What makes multi-modal learning better than single (provably), 2021.
- [23] Norman Lloyd Johnson, Samuel Kotz, and Narayanaswamy Balakrishnan. *Continuous multivariate distributions*, volume 7. Wiley New York, 1972.
- [24] Audun Jsang. *Subjective Logic: A formalism for reasoning under uncertainty*. Springer Publishing Company, Incorporated, 2018.
- [25] Anna-Kathrin Kopetzki, Bertrand Charpentier, Daniel Zügner, Sandhya Giri, and Stephan Günnemann. Evaluating robustness of predictive uncertainty estimation: Are dirichlet-based models reliable? In *International Conference on Machine Learning*, pages 5707–5718. PMLR, 2021.
- [26] Hong Li, Xingyu Li, Pengbo Hu, Yinuo Lei, Chunxiao Li, and Yi Zhou. Boosting multi-modal model performance with adaptive gradient modulation. In *Proceedings of the IEEE/CVF International Conference on Computer Vision*, pages 22214–22224, 2023.
- [27] Yikuan Li, Shishir Rao, José Roberto Ayala Solares, Abdelaali Hassaine, Rema Ramakrishnan, Dexter Canoy, Yajie Zhu, Kazem Rahimi, and Gholamreza Salimi-Khorshidi. Behrt: transformer for electronic health records. *Scientific reports*, 10(1):7155, 2020.
- [28] David JC MacKay. Bayesian interpolation. *Neural computation*, 4(3):415–447, 1992.
- [29] Andrey Malinin and Mark Gales. Predictive uncertainty estimation via prior networks. *Advances in neural information processing systems*, 31, 2018.
- [30] Andrey Malinin, Bruno Mlodozienec, and Mark Gales. Ensemble distribution distillation. *arXiv preprint arXiv:1905.00076*, 2019.
- [31] Bjoern H Menze, Andras Jakab, Stefan Bauer, Jayashree Kalpathy-Cramer, Keyvan Farahani, Justin Kirby, Yuliya Burren, Nicole Porz, Johannes Slotboom, Roland Wiest, et al. The multimodal brain tumor image segmentation benchmark (brats). *IEEE transactions on medical imaging*, 34(10):1993–2024, 2014.
- [32] Thomas P Minka. Expectation propagation for approximate bayesian inference. *arXiv preprint arXiv:1301.2294*, 2013.
- [33] Thomas Peter Minka. *A family of algorithms for approximate Bayesian inference*. PhD thesis, Massachusetts Institute of Technology, 2001.
- [34] Ghulam Muhammad, Fatima Alshehri, Fakhri Karray, Abdulmotaleb El Saddik, Mansour Alsulaiman, and Tiago H Falk. A comprehensive survey on multimodal medical signals fusion for smart healthcare systems. *Information Fusion*, 76:355–375, 2021.
- [35] Arsha Nagrani, Shan Yang, Anurag Arnab, Aren Jansen, Cordelia Schmid, and Chen Sun. Attention bottlenecks for multimodal fusion. *Advances in neural information processing systems*, 34:14200–14213, 2021.
- [36] Radford M Neal. *Bayesian learning for neural networks*, volume 118. Springer Science & Business Media, 2012.
- [37] Jiquan Ngiam, Aditya Khosla, Mingyu Kim, Juhan Nam, Honglak Lee, Andrew Y Ng, et al. Multimodal deep learning. In *ICML*, volume 11, pages 689–696, 2011.

- [38] Athanasios Papoulis. *Random variables and stochastic processes*. McGraw Hill, 1965.
- [39] Xiaokang Peng, Yake Wei, Andong Deng, Dong Wang, and Di Hu. Balanced multimodal learning via on-the-fly gradient modulation. In *Proceedings of the IEEE/CVF conference on computer vision and pattern recognition*, pages 8238–8247, 2022.
- [40] Soujanya Poria, Erik Cambria, Rajiv Bajpai, and Amir Hussain. A review of affective computing: From unimodal analysis to multimodal fusion. *Information fusion*, 37:98–125, 2017.
- [41] Soujanya Poria, Erik Cambria, and Alexander Gelbukh. Deep convolutional neural network textual features and multiple kernel learning for utterance-level multimodal sentiment analysis. In *Proceedings of the 2015 conference on empirical methods in natural language processing*, pages 2539–2544, 2015.
- [42] John A Rice and John A Rice. *Mathematical statistics and data analysis*, volume 371. Thomson/Brooks/Cole Belmont, CA, 2007.
- [43] Christian P Robert, George Casella, and George Casella. *Monte Carlo statistical methods*, volume 2. Springer, 1999.
- [44] Ozan Sener and Vladlen Koltun. Multi-task learning as multi-objective optimization. *Advances in neural information processing systems*, 31, 2018.
- [45] Murat Sensoy, Lance Kaplan, and Melih Kandemir. Evidential deep learning to quantify classification uncertainty. *Advances in neural information processing systems*, 31, 2018.
- [46] Yao-Hung Hubert Tsai, Shaojie Bai, Paul Pu Liang, J Zico Kolter, Louis-Philippe Morency, and Ruslan Salakhutdinov. Multimodal transformer for unaligned multimodal language sequences. In *Proceedings of the conference. Association for computational linguistics. Meeting*, volume 2019, page 6558. NIH Public Access, 2019.
- [47] Hu Wang, Congbo Ma, Jianpeng Zhang, Yuan Zhang, Jodie Avery, Louise Hull, and Gustavo Carneiro. Learnable cross-modal knowledge distillation for multi-modal learning with missing modality. In *International Conference on Medical Image Computing and Computer-Assisted Intervention*, pages 216–226. Springer, 2023.
- [48] Jingyao Wang, Luntian Mou, Lei Ma, Tiejun Huang, and Wen Gao. Amsa: Adaptive multimodal learning for sentiment analysis. *ACM Transactions on Multimedia Computing, Communications and Applications*, 19(3s):1–21, 2023.
- [49] Jingyao Wang, Luntian Mou, Changwen Zheng, and Wen Gao. Image-based freeform handwriting authentication with energy-oriented self-supervised learning. *arXiv preprint arXiv:2408.09676*, 2024.
- [50] Jingyao Wang, Siyu Zhao, Wenwen Qiang, Jiangmeng Li, Fuchun Sun, and Hui Xiong. On the causal sufficiency and necessity of multi-modal representation learning, 2025.
- [51] Weiyao Wang, Du Tran, and Matt Feiszli. What makes training multi-modal classification networks hard? In *Proceedings of the IEEE/CVF conference on computer vision and pattern recognition*, pages 12695–12705, 2020.
- [52] Yake Wei and Di Hu. Mmpareto: Boosting multimodal learning with innocent unimodal assistance. In *Forty-first International Conference on Machine Learning*, 2024.
- [53] Max Welling and Yee W Teh. Bayesian learning via stochastic gradient langevin dynamics. In *Proceedings of the 28th international conference on machine learning (ICML-11)*, pages 681–688. Citeseer, 2011.
- [54] Christopher KI Williams and Carl Edward Rasmussen. *Gaussian processes for machine learning*, volume 2. MIT press Cambridge, MA, 2006.
- [55] Nan Wu, Stanislaw Jastrzebski, Kyunghyun Cho, and Krzysztof J Geras. Characterizing and overcoming the greedy nature of learning in multi-modal deep neural networks. In *International Conference on Machine Learning*, pages 24043–24055. PMLR, 2022.
- [56] Peng Xu, Timothy M Hospedales, Qiyue Yin, Yi-Zhe Song, Tao Xiang, and Liang Wang. Deep learning for free-hand sketch: A survey. *IEEE transactions on pattern analysis and machine intelligence*, 45(1):285–312, 2022.
- [57] Xiaodong Yue, Zhicheng Dong, Yufei Chen, and Shaorong Xie. Evidential dissonance measure in robust multi-view classification to resist adversarial attack. *Information Fusion*, 113:102605, 2025.

- [58] Yao Zhang, Nanjun He, Jiawei Yang, Yuexiang Li, Dong Wei, Yawen Huang, Yang Zhang, Zhiqiang He, and Yefeng Zheng. mmformer: Multimodal medical transformer for incomplete multimodal learning of brain tumor segmentation. In *International Conference on Medical Image Computing and Computer-Assisted Intervention*, pages 107–117. Springer, 2022.

Appendix

The appendix is organized into several sections:

- Appendix A provides the detailed proofs of the theorem in the main text.
- Appendix B provides details for all notations used in this paper.
- Appendix C provides more discussion about the proposed methodology.
- Appendix D provides details for the benchmark datasets used in the experiments.
- Appendix E provides details for the baselines mentioned in the main text.
- Appendix F contains details for the implementation of the experiment.
- Appendix G provides the full results and analyses of the experiment.

A Proofs

Proof. Given a Gaussian prior $\theta \sim \mathcal{N}(\mu_0, \frac{1}{\lambda_0})$ with the mean θ , where $\lambda_0 > 0$ is the precision. Given n observations x_1, \dots, x_n with known noise precision $\tau > 0$, the likelihood is $p(x_{1:n} | \theta) = \prod_{i=1}^n \mathcal{N}(x_i | \theta, \frac{1}{\tau})$. The prior density is $p(\theta) = \sqrt{\frac{\lambda_0}{2\pi}} \exp[-\frac{\lambda_0}{2}(\theta - \mu_0)^2]$ and the likelihood factorizes as $p(x_{1:n} | \theta) = \prod_{i=1}^n \sqrt{\frac{\tau}{2\pi}} \exp[-\frac{\tau}{2}(x_i - \theta)^2]$. According to Bayes' rule, we can obtain $p(\theta | x_{1:n}) \propto p(\theta)p(x_{1:n} | \theta)$. Hence, we can derive

$$p(\theta | x_{1:n}) \propto \exp[-\frac{\lambda_0}{2}(\theta - \mu_0)^2 - \frac{\tau}{2} \sum_{i=1}^n (\theta - x_i)^2] \quad (18)$$

Then, we expand the sum of squares:

$$\begin{aligned} \lambda_0(\theta - \mu_0)^2 + \tau \sum_{i=1}^n (\theta - x_i)^2 &= \lambda_0(\theta^2 - 2\mu_0\theta + \mu_0^2) + \tau \sum_{i=1}^n (\theta^2 - 2x_i\theta + x_i^2) \\ &= (\lambda_0 + n\tau)\theta^2 - 2(\lambda_0\mu_0 + \tau \sum_{i=1}^n x_i)\theta + (\lambda_0\mu_0^2 + \tau \sum_{i=1}^n x_i^2), \end{aligned} \quad (19)$$

Define $\lambda_n = \lambda_0 + n\tau$, $\mu_n = \frac{\lambda_0\mu_0 + \tau \sum_{i=1}^n x_i}{\lambda_n}$. Then the exponent becomes

$$\lambda_n(\theta^2 - 2\mu_n\theta + \mu_n^2) + \underbrace{(\lambda_0\mu_0^2 + \tau \sum_{i=1}^n x_i^2 - \lambda_n\mu_n^2)}_{\text{const. w.r.t } \theta} \quad (20)$$

Ignoring the additive constant, we can obtain $p(\theta | x_{1:n}) \propto \exp[-\frac{\lambda_n}{2}(\theta - \mu_n)^2]$. Thus, the posterior is Gaussian with updated precision $\lambda_n = \lambda_0 + n\tau$ as follows:

$$\theta | x_{1:n} \sim \mathcal{N}(\mu_n, \frac{1}{\lambda_n}), \quad (21)$$

where λ_n objectively measures the total information accumulated from prior and n data points.

Given an exponent $s \in \mathbb{R}^+$, we define a power mapping as follows:

$$\phi : (0, \infty) \rightarrow (0, \infty), \quad \phi(\lambda) = (\lambda)^s, \quad (22)$$

where ϕ has three properties and we'll verify them next.

First, ϕ has monotonicity, i.e. given any $\lambda_2 > \lambda_1 > 0$, $\phi(\lambda_2) > \phi(\lambda_1)$. Since $s > 0$, the function $\phi(\lambda) = (\lambda)^s$ has derivative

$$\phi'(\lambda) = s(\lambda)^{s-1}, \quad \forall \lambda > 0, \quad (23)$$

A continuously differentiable function whose derivative is strictly positive is strictly increasing. Thus, $\lambda_2 > \lambda_1 \Rightarrow \lambda_2^s > \lambda_1^s$.

Second, ϕ control amplification or attenuation through s . Compute the second derivative:

$$\phi''(\lambda) = s(s-1)\lambda^{s-2}, \quad (24)$$

Table 4: The definitions of notations

Notations	Definitions
<i>Notations of Data</i>	
\mathcal{X}, \mathcal{Y}	The input space and label space
$(x_t, y_t) \in \mathcal{X} \times \mathcal{Y}$	The t -th sample $x_t \in \mathcal{X}$ and the label $y_t \in \mathcal{Y}$
$D^i = \{(x_t^i, y_t^i)\}_{t=1}^n$	The dataset of the i -th modality with n samples
$\mathcal{D}_{batch} \sim \mathcal{D}$	The random batch of samples
$x_t = \{x_t^1, \dots, x_t^{(i)}\}$	Each sample, which contains M modalities
Δ^{K-1}	The K -dimensional unit simplex
<i>Notations of Model</i>	
$f_{\Theta}: \mathcal{X} \rightarrow \mathcal{Y}$	The MML model
ψ_t	The shared hidden layer of MML model
Θ	Parameters of the last layer before output
<i>Notations of Variables</i>	
X, Y	Variables of the sample and corresponding label
\hat{Y}	The network output
M	The total number of modalities
μ, Σ	Mean and covariance matrix of gradient distribution
μ_t^i, Σ_t^i	Mean and covariance matrix of gradient distribution \mathbf{g}_t^i of the i -th modality for the t -th sample
$(\sigma_t^i)^2$	The variance of the covariance matrix Σ_t^i
$\Lambda_t^i := \frac{1}{\Sigma_t^i}$	The precision of gradient distribution \mathbf{g}_t^i of the i -th modality for the t -th sample
$\lambda_{t,d}^i$	The precision of the gradient distribution \mathbf{g}_t^i of the i -th modality for the t -th sample in the d -th dimension
$(\Sigma_t^i)^{-1}[d, d]$	The element of the d -th row and d -th column in Λ_t^i
$e_{t,d}^i, b_{t,d}^i$	The evidence and belief of the gradient distribution \mathbf{g}_t^i of the i -th modality for the t -th sample in the d -th dimension
u_t^i	The uncertainty of gradient distribution \mathbf{g}_t^i of the i -th modality for the t -th sample
α	The concentration parameters of Dirichlet distribution
$\mathbb{M} = \{b, u\}$	The set of masses including belief and uncertainty
S	The Dirichlet strength
C	The measure of the amount of conflict between the two mass sets
<i>Notations of Learning Objective</i>	
$\mathcal{L}_{\text{fusion}}$	The multi-modal fusion loss that aggregates information from all modalities
$\mathcal{L}_{\text{uni}}^i$	The loss for the individual i -th modality
$\mathcal{L} = (Y - \hat{Y})^2$	The standard square loss between label Y and network output \hat{Y}
\mathbf{g}_t^i	Gradient distribution of the i -th modality for the t -th sample
$\mathbf{g}_{\text{fusion}}^i$	Gradient distribution of the multi-modal fusion loss
\mathbf{g}_{DS}	Gradient update direction obtained by Bayesian method

If $s > 1$, then $s(s-1) > 0$, $\phi''(\lambda) > 0$, so ϕ is convex. If $0 < s < 1$, then $s(s-1) < 0$, $\phi''(\lambda) < 0$, so ϕ is concave.

For convex ϕ , the secant slope exceeds the tangent at the left endpoint:

$$\frac{\phi(\lambda_2) - \phi(\lambda_1)}{\lambda_2 - \lambda_1} > \phi'(\lambda_1) = s\lambda_1^{s-1}, \quad (25)$$

Multiplying both sides by $\lambda_2 - \lambda_1 > 0$ yields $\phi(\lambda_2) - \phi(\lambda_1) > s\lambda_1^{s-1}(\lambda_2 - \lambda_1)$, so the differences in λ are amplified when $s > 1$.

For concave ϕ , the reverse inequality holds $\phi(\lambda_2) - \phi(\lambda_1) < s\lambda_1^{s-1}(\lambda_2 - \lambda_1)$, so the differences in λ are attenuated when $0 < s < 1$.

Third, we discuss the boundary behaviors of ϕ . Specifically, as $\lambda \rightarrow 0^+$, $\lim_{\lambda \rightarrow 0^+} \lambda^s = 0^s = 0$. This interprets that with no information ($\lambda \rightarrow 0$), evidence $e \rightarrow 0$. As $\lambda \rightarrow +\infty$, $\lim_{\lambda \rightarrow +\infty} \lambda^s = +\infty$. This interprets that with unbounded information, evidence grows unbounded.

These three points establish that defining evidence by the power mapping is both mathematically valid (positive and strictly increasing) and semantically meaningful (treating precision as effective sample size and permitting controlled scaling).

B Notation

In this section, we briefly describe the symbols that we mainly use in this article. In table 4, we give the definitions of notation according to their role.

C More Discussion

C.1 Illustration of Important Concepts

C.1.1 Bayesian Inference

Bayesian inference represents and manages uncertainty by constructing probabilistic models. In Bayesian inference [8, 14], uncertainty is described using probability distributions that reflect the degree of belief in different possible values of a variable or parameter. Bayesian inference provides a principled foundation for reasoning under uncertainty, and has been widely adopted in machine learning to quantify model confidence [8, 14]. The key idea is to treat model parameters as random variables and to update our belief about them after observing data. This update is formalized by Bayes' theorem

$$p(\Theta | \mathcal{D}) = \frac{p(\mathcal{D} | \Theta)p(\Theta)}{p(\mathcal{D})} \quad (26)$$

where $p(\Theta)$ is the prior distribution encoding our initial belief about the parameters Θ , $p(\mathcal{D} | \Theta)$ is the likelihood of observing the data given the parameters, and $p(\Theta | \mathcal{D})$ is the resulting posterior after incorporating evidence from the data.

C.1.2 Dirichlet Distribution

The Dirichlet distribution is a continuous probability distribution defined on a K -dimensional unit simplex $\Delta^{K-1} = \{\mathbf{z} = (z_1, \dots, z_K) \mid z_n > 0, \sum_{n=1}^K z_n = 1\}$ [7]. The probability density function of the Dirichlet distribution is as follows:

$$Dir(\mathbf{z} | \boldsymbol{\alpha}) = \frac{1}{B(\boldsymbol{\alpha})} \prod_{n=1}^K z_n^{\alpha_n - 1} \quad (27)$$

where $\boldsymbol{\alpha} = [\alpha_1, \dots, \alpha_K]$ are concentration parameters of the Dirichlet distribution, $B(\boldsymbol{\alpha})$ is the K -dimensional multinomial beta function [23].

In multi-modal classification, given a multi-modal observation $\mathbf{x} = \{x^i\}_{i=1}^M$, $\mathbf{x} \in \mathcal{X}$ and the label $\mathbf{y} \in \mathcal{Y}$, where \mathcal{X} is the set of all observations and \mathcal{Y} is the set of all labels. Given the i -th modality, the generative process is as follows:

$$\mathbf{z}^i \sim Dir(\mathbf{z}^i | \boldsymbol{\alpha}^i), \quad \mathbf{y} \sim Mult(\mathbf{y} | \mathbf{z}^i) \quad (28)$$

where $Mult(\mathbf{y} | \mathbf{z}^i)$ is a multinomial distribution and $\mathbf{z}^i = [z_1^i, \dots, z_1^i]$ are the parameters of the multinomial distribution.

C.2 More Illustration of Figure 1

The left (green) panel of Figure 1 juxtaposes two kinds of gradient aggregation strategies: (i) deterministic gradient aggregation, where modality gradients are combined via fixed or dynamically learned scalar weights or multi-objective optimization to find a compromise direction, and (ii) uncertainty driven gradient aggregation, which first estimates uncertainty of each modality gradient and then utilizes these uncertainties to guide the MML optimization. The right (yellow) panel of Figure 1 provides the widely used MML optimization framework. Specifically, the input of each modality is passed through its dedicated encoder and merged into a shared hidden representation. Then, both the fusion loss and individual modality losses are computed. During backpropagation, we obtain both individual modality gradients and the standard fusion gradient. These gradients are merged into an update direction via a specific aggregation strategy. Finally, the aggregated gradient is applied through the optimizer (e.g. SGD or Adam) to update the parameters of MML network.

Compared with the deterministic gradient aggregation strategy, the optimal direction of the uncertainty driven gradient aggregation strategy is located at the highest density point of the two gradient distributions. This means that the optimal direction corresponds to the most probable gradient direction under both modality distributions simultaneously, ensuring the update step is the direction that best explains all available evidence. If a modality gradient exhibits fluctuations or outliers in specific dimensions, the uncertainty driven gradient aggregation strategy naturally shifts weight toward the other modality with more reliable estimates, attenuating the influence of noisy signals.

C.3 Derivations of Posterior Approximation

In this subsection, we provide the derivation of Eq.6. First, we define and recap some notations here.

$$p = \log p(\Theta | \mathcal{D}), \mathbf{q} = -\nabla_{\Theta} \log p(\mathcal{D}, \Theta), \mathbf{H} = -\nabla_{\Theta}^2 \log p(\mathcal{D}, \Theta) \quad (29)$$

According to Eq.5, we use the above notations to obtain the following form:

$$\begin{aligned} & p + \mathbf{q}^\top (\Theta - \hat{\Theta}) + \frac{1}{2} (\Theta - \hat{\Theta})^\top \mathbf{H} (\Theta - \hat{\Theta}) \\ &= p - \mathbf{q}^\top \hat{\Theta} + \underbrace{\frac{1}{2} (\hat{\Theta}^\top \mathbf{H} \hat{\Theta}) - (\mathbf{H}^\top \hat{\Theta} - \mathbf{q})^\top \mathbf{H}^{-1} (\mathbf{H}^\top \hat{\Theta} - \mathbf{q})}_{const.} \\ &+ \frac{1}{2} (\Theta - (\hat{\Theta} - \mathbf{H}^{-1} \mathbf{q}))^\top \mathbf{H} (\Theta - (\hat{\Theta} - \mathbf{H}^{-1} \mathbf{q})) \end{aligned} \quad (30)$$

The above takes the quadratic form of a Gaussian having mean $(\hat{\Theta} - \mathbf{H}^{-1} \mathbf{q})$ and covariance \mathbf{H}^{-1} .

C.4 Explanation of Steps within BOGC-MML

In this subsection, we provide more explanations about our proposed method.

Why can Eq.5 be expressed in this way. According to the Laplace approximation [28], Eq.5 conforms to the second-order Taylor expansion, i.e. $f(\mathbf{x}) \approx f(\hat{\mathbf{x}}) + \nabla f(\hat{\mathbf{x}})^\top (\mathbf{x} - \hat{\mathbf{x}}) + \frac{1}{2} (\mathbf{x} - \hat{\mathbf{x}})^\top \mathbf{H}_f(\hat{\mathbf{x}}) (\mathbf{x} - \hat{\mathbf{x}})$.

Why is the first-order term of Eq.5 omitted. In Eq.5, we expand the log-posterior around the learned point estimate $\hat{\Theta}^i$. The first-order term $(-\nabla_{\Theta^i} \log p(\mathcal{D}, \Theta^i))^\top \Delta \Theta^i$ is omitted because the gradient of the joint log-density vanishes, i.e. $\nabla_{\Theta^i} \log p(\mathcal{D}, \Theta^i)|_{\Theta^i = \hat{\Theta}^i} = 0$. Thus, when expanding around a stationary point, the Jacobian term is identically zero and contributes nothing to the approximation.

How can the gradient distribution of each modality be calculated through the first and second-order moments. By matching the first and second-order moments, we can obtain the Gaussian distribution that, among all Gaussian distributions, is closest in the sense of Kullback-Leibler divergence to the true distribution of the gradients [32]. In other words, we preserve as much of the original distribution shape as possible by forcing it into Gaussian form.

Why α equals $e + 1$. According to subjective logic [24] and evidence theory [6, 45], each Dirichlet concentration parameter α represents a "pseudo-count", while the actual observed evidence is denoted e . To ensure a non-informative prior when no evidence is available, the initial pseudo-count is usually selected as 1 [24]. Consequently, we can obtain $\alpha = e + 1$.

Note that the

C.5 More Comparison

In this subsection, we further discuss the differences between BOGC-MML and the previous or concurrent methods.

Recently, optimization methods using a combination of multi-modal fusion loss and multiple unimodal losses have achieved promising performance [51]. Many methods focus on how to obtain multi-modal fusion losses through new strategies or how to aggregate multi-modal fusion losses with unimodal losses to obtain updated directions [39, 44, 46, 49, 51, 52]. However, these methods usually regard the lost gradient as deterministic values. Unlike previous MML methods, our proposed BOGC-MML presents a novel optimization framework. Specifically, we focus on how to model the probability distributions of multi-modal fusion loss and unimodal losses, and then how to use the probability distributions for gradient aggregation to obtain the updated direction.

For uncertainty-based learning, although the existing neural networks are effective in many fields, most neural networks rely on deterministic functions, so the uncertainties in neural networks are difficult to obtain. To address these uncertainties, several methods have been developed. Recently, methods based on subjective logic [24] and Dempster-Shafer evidence theory [15] have shown promise in uncertainty estimation. Unlike methods indirectly model uncertainty through network

weights, these methods have been successively proposed to directly model uncertainty [10, 25, 29, 30, 45]. Despite recent efforts to improve MML model performance, these approaches typically consider modality gradients as deterministic values and struggle to quantify the uncertainty of modality gradients. To this end, we propose a novel calibration framework that quantifies and aggregate uncertainties of modality gradients to calibrate the update direction in MML optimization. We also compare our method with the previous uncertainty-focused methods, where experimental results demonstrate our advantages.

C.6 Boarder Impacts and Limitations

In this subsection, we briefly illustrate the broader impacts and limitations of this work.

Boarder Impacts. This work introduce BOGC-MML, a Bayesian-oriented gradient calibration framework that explicitly models and aggregates the uncertainty of modality-specific gradients during MML optimization. Our empirical results demonstrate that the proposed method achieve validity across diverse benchmarks. This work bridges Bayesian inference, evidence theory, and gradient-based optimization, offering a blueprint for future work on uncertainty-aware training regimes across machine learning disciplines.

Limitations. This work evaluates BOGC-MML mainly on supervised tasks where loss gradients are driven by explicit ground-truth labels. However, we have not explored how uncertainty-calibrated gradient aggregation behaves in unsupervised or self-supervised settings, such as clustering, generative modeling, or contrastive representation learning without labels. We will investigate additional case studies to extend this work in the future.

D Benchmark Datasets

In this section, we provide a brief overview of the benchmark datasets used in our experiments.

- CREMA-D [9] is a multimodal emotion recognition dataset designed to study how humans perceive emotions through audio, visual, and audiovisual stimuli. It contains 7,442 clips from 91 actors (48 male, 43 female) of diverse racial and ethnic backgrounds (African American, Asian, Caucasian, Hispanic, etc.). Actors performed 12 sentences in six basic emotions (Anger, Disgust, Fear, Happy, Neutral, Sad) across four intensity levels (Low, Medium, High, Unspecified). Each clip was rated by 2,443 crowd-sourced participants in three modalities: audio-only, video-only, and audiovisual. The dataset includes annotations for emotion categories, intensity levels, and actor demographics (age, sex, race, ethnicity).
- Kinetics Sounds [3] is a subset of the Kinetics-600 dataset, curated for audio-visual action recognition. It focuses on human actions with distinctive sound cues, such as playing musical instruments, cooking, or sports. The dataset includes 19,000 video clips (10 seconds each) across 31 action classes, derived from YouTube. Each clip is annotated with temporal and semantic labels for both audio and visual modalities. It is widely used to benchmark models that fuse audio and visual features for tasks like action classification and event detection.
- BraTS [31] is a multimodal medical imaging dataset for brain tumor segmentation. While not explicitly detailed in the provided search results, it is widely recognized in medical AI research. The dataset includes multiparametric MRI scans (T1, T1c, T2, FLAIR) from glioblastoma patients, annotated with tumor sub-regions (enhancing tumor, tumor core, whole tumor). It is used in annual challenges to benchmark segmentation algorithms under missing or incomplete modalities[citation:Table in user’s previous query].

E Baselines

In this section, we provide a brief overview of the baselines used for comparison in our experiments.

- G-Blending [51] proposes gradient blending to dynamically adjust modality-specific gradients during training. It mitigates modality competition by reweighting gradients based on their contributions, improving worst-case accuracy.

- Occlusion-guided Modulation (OGM) [39] adaptively modulates modality-specific learning speeds based on their relative contributions. It suppresses over-confident modalities to encourage balanced learning. While improving robustness, its unimodal performance drops significantly due to suppressed modality-specific features.
- Greedy [55] propose a modality selection strategy that greedily optimizes the primary modality while neglecting the weaker one. This leads to severe video performance degradation, highlighting the risk of modality collapse in imbalanced settings.
- Probability Margin Regularization (PMR) [17] enforces a margin between correct and incorrect class probabilities to reduce modality overconfidence. However, its overly strict constraints harm video modality learning, suggesting limited adaptability to severe imbalance.
- Adaptive Gradient Modulation (AGM) [26] dynamically adjusts gradient magnitudes for each modality based on their training status. While moderately improving worst-case accuracy, it struggles to balance modality-specific and joint representation learning.
- Trusted Modality Combination (TMC) [20] introduces a trusted modality combination (TMC) mechanism that first estimates a reliability score for each modality via a data-driven trust model, then weights modality gradients according to these scores during fusion.
- Evidential Confictive Multi-view Learning (ECML) [57] leverages evidential calibration to convert each modality’s predictive uncertainty into Dempster-Shafer evidence; these evidence masses are used to derive fusion weights that reflect both confidence and uncertainty.
- MMPareto [52] is a multi-objective optimization framework that seeks Pareto-optimal solutions for modality balance. It achieves strong results by optimizing accuracy and fairness simultaneously. Its Pareto-efficient training ensures no modality is severely neglected.

In addition, for the missing modality scenario, we select several strong baseline as comparison baselines.

- Hierarchical Multi-modal Image Segmentation (HMIS) [21] is a traditional or early deep learning-based method for multi-modal medical image segmentation. It typically employs a hierarchical architecture to process multi-modal inputs sequentially or in parallel. When modalities are missing, HMIS may rely on simple heuristics (e.g., interpolation, modality replacement) or statistical imputation to fill gaps. However, its performance degrades significantly under extreme missing-modality scenarios due to limited adaptability. It serves as a foundational baseline for comparing robustness against modality incompleteness.
- Recurrent Segmentation Network (RSeg) [11] leverages recurrent neural networks (RNNs) or attention-based recurrent mechanisms to iteratively refine segmentation predictions. It is designed to handle sequential dependencies between modalities or spatial regions. For missing modalities, RSeg might use learned memory cells or attention gates to compensate for absent data. While effective in capturing temporal/spatial relationships, its performance depends heavily on the quality of modality-specific feature extraction and may struggle with highly heterogeneous missing patterns.
- Multi-modal Feature Memory (mmFm) [58] introduces a memory-augmented network that stores modality-specific features in a shared memory bank. During inference, the model retrieves and combines features from the memory to compensate for missing modalities. This approach explicitly models cross-modal correlations and leverages stored patterns to handle incomplete inputs. However, its effectiveness relies on the diversity of the training data and may fail when encountering unseen missing-modality combinations.
- Latent Cross-Modal Knowledge Distillation (LCKD) [47] employs knowledge distillation to transfer knowledge from a teacher model (trained on complete modalities) to a student model that handles missing modalities. The latent representations of the teacher guide the student to mimic robust features even when specific modalities are absent. This method mitigates performance drops by enforcing consistency in latent space but requires a two-stage training process and may suffer from information loss during distillation.

Table 5: Classification accuracy(%) on CREMA-D and Kinetics Sounds. The best results are shown in **bold**. * indicates that the unimodal accuracy (Acc audio and Acc video) is obtained by fine-tuning a unimodal classifier with the trained unimodal encoder frozen.

Method	CREMA-D				Kinetics Sounds			
	Acc	Acc audio	Acc video	Worst Acc	Acc	Acc audio	Acc video	Worst Acc
Audio-only	-	61.69	-	-	-	53.63	-	-
Video-only	-	-	56.05	-	-	-	49.20	-
Unimodal pre-trained & fine-tune	71.51	60.08	60.22	68.51	68.75	53.49	50.07	66.75
One joint loss*	66.13	59.27	36.56	63.63	64.61	52.03	35.47	61.61
Uniform baseline	71.10	63.44	51.34	69.30	68.31	53.20	40.55	66.11
G-Blending [51]	72.01	60.62	52.23	69.31	68.90	52.11	41.35	65.40
OGM [39]*	69.19	56.99	40.05	66.89	66.79	51.09	37.86	64.90
Greedy [55]*	67.61	60.69	38.17	65.51	65.32	50.58	35.97	62.52
PMR [17]*	66.32	59.95	32.53	64.62	65.70	52.47	34.52	62.30
AGM [26]*	70.06	60.38	37.54	68.06	66.17	51.31	34.83	63.67
TMC [20]	72.84 \pm 0.98	61.73 \pm 1.02	52.25 \pm 0.88	69.76 \pm 0.93	70.17 \pm 1.12	55.53 \pm 0.86	50.83 \pm 1.21	67.64 \pm 0.82
ECML [57]	74.68 \pm 1.17	62.31 \pm 0.95	53.16 \pm 0.83	70.77 \pm 1.07	71.25 \pm 1.17	56.24 \pm 0.95	51.35 \pm 1.17	68.08 \pm 0.87
MMPareto [52]	75.13	65.46	55.24	71.93	70.13	56.40	53.05	67.33
Ours	78.91 \pm 0.78	68.52 \pm 0.85	58.79 \pm 0.59	74.02 \pm 0.76	72.64 \pm 0.82	58.11 \pm 0.79	56.89 \pm 0.91	69.37 \pm 0.65

F Implementation Details

Unless otherwise specified, our experiments utilize a ResNet-18 backbone, and all models are trained from scratch without pre-trained weights. We learn the parameters of the last layer as part of the posterior approximation. Moving on to the optimization process, we use SGD with momentum (0.9) and $\gamma = 1.5$ in experiments. The initial learning rate is set to 0.1 and can be linearly scaled if needed. We also determine the hyperparameter s through grid search, resulting in $s = 0.5$. We have constructed dedicated ablation experiments for the selection of these parameters. Experimental results demonstrate that the model maintains relatively stable performance across different datasets under various hyperparameter settings. For evaluation, the training dataset is randomly split into training and validation sets. Hyperparameters are tuned on the validation set to maximize performance, and final accuracy is reported on the test dataset. All experiments are conducted over five runs using NVIDIA Tesla V100 GPUs.

G Full Experimental Results and Analyses

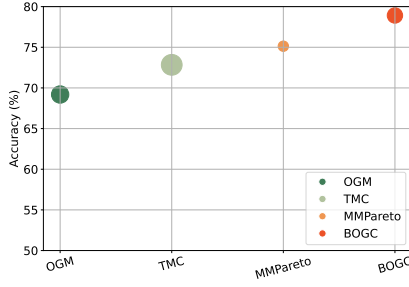
G.1 Performance Comparison

The results are shown in Table 1. From the results, we can observe that our approach achieves optimal performance, outperforming both unimodal and multimodal methods. Specifically, the uniform baseline (where all loss weights are equal) demonstrates strong competitiveness in multimodal learning tasks, especially in unimodal evaluations. For example, on the CREMA-D dataset, the uniform baseline achieves an audio accuracy of 63.44% and a video accuracy of 51.34%, surpassing some multimodal methods specifically designed to address modality imbalance, such as OGM, Greedy, PMR, and AGM. This suggests that balancing multimodal losses alone, without additional complex optimization strategies, can serve as a strong baseline. This may be because it prevents excessive optimization of a single modality, ensuring balanced learning across modalities. Building on this foundation, our method further enhances multimodal learning performance, achieving the best results across all evaluation metrics, further proving its superiority. Moreover, compared to the best multimodal MMPareto, our method shows additional improvements, particularly in unimodal tasks. For instance, on the CREMA-D dataset, the audio accuracy increases from 65.46% to 68.02%, and the video accuracy improves from 55.24% to 56.39%. This demonstrates that our optimization approach further enhances Pareto-based performance and highlights the importance of dimensional uncertainty.

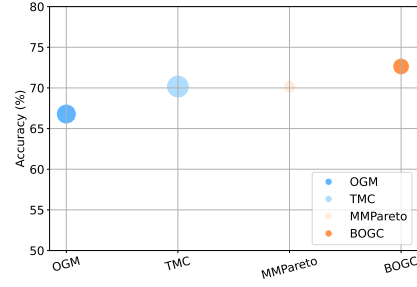
Further, **Table 2** shows the performance analysis compares a transformer-based framework (MBT) on the CREMA-D and Kinetics Sounds datasets, evaluating accuracy (Acc) and macro F1-score under two training setups: from scratch and with pretraining. Our method achieves the best results, with CREMA-D reaching 74.00% accuracy (pretraining) and Kinetics Sounds achieving 73.17% accuracy (pretraining), significantly outperforming baselines like MMPareto and uniform baseline. Pretraining notably enhances performance across all methods, with our approach showing the most improvement, underscoring its effectiveness in addressing modality imbalance and leveraging pre-trained features. This demonstrates the robustness of BOGC-MML in multimodal learning.

Table 6: Test performance on CREMA-D and Kinetics Sounds where **bold** and underline represent the best and runner-up respectively. The network follows transformer-based framework MBT [35].

Method	CREMA-D				Kinetics Sounds			
	from scratch		with pretrain		from scratch		with pretrain	
	Acc	macro F1	Acc	macro F1	Acc	macro F1	Acc	macro F1
One joint loss	44.96	42.78	66.69	67.26	42.51	41.56	68.30	69.31
Uniform baseline	45.30	43.74	69.89	70.11	43.31	43.08	69.40	69.60
G-Blending [51]	46.38	45.16	69.91	70.01	44.69	44.19	69.41	69.47
OGM-GE [39]	42.88	39.34	65.73	65.88	41.79	41.09	69.55	69.53
Greedy [55]	44.49	42.76	66.67	67.26	43.31	43.08	69.62	69.75
PMR [17]	44.76	42.95	65.59	66.07	43.75	43.21	69.67	69.87
AGM [26]	45.36	43.81	66.54	67.75	43.65	43.57	69.59	69.14
TMC [20]	46.83 \pm 0.83	46.26 \pm 0.93	68.96 \pm 0.85	69.61 \pm 1.02	43.91 \pm 0.79	43.95 \pm 0.84	69.02 \pm 0.69	68.56 \pm 0.72
ECML [57]	48.00 \pm 0.78	47.26 \pm 0.97	70.11 \pm 0.69	70.86 \pm 0.95	45.13 \pm 0.74	44.75 \pm 0.93	70.12 \pm 0.82	69.61 \pm 0.92
MMPareto [52]	<u>48.66</u>	<u>48.17</u>	<u>70.43</u>	<u>71.17</u>	<u>45.20</u>	<u>45.26</u>	<u>70.28</u>	<u>70.11</u>
Ours	52.21 \pm 0.69	50.06 \pm 0.74	74.00 \pm 0.78	73.01 \pm 0.83	47.19 \pm 0.68	47.36 \pm 0.86	73.17 \pm 0.79	74.08 \pm 0.83



(a) Result on CREMA-D



(b) Result on Kinetics Sounds

Figure 4: Trade-off performance of various methods, with point size reflecting training time.

In addition, Tables 5 and 6 provide more detailed experimental results, including performance metrics with standard deviations. Results without standard deviations are taken from the original literature, while those with standard deviations are obtained from our reproduced implementations.

G.2 Trade-off Performance

We further investigate the trade-off between model performance and computational efficiency. Under the same backbone, we compare several baseline methods, including OGM, TMC, MMPareto, and BOGC, on the CREMA-D dataset. As shown in Figure 4, the vertical axis represents classification accuracy (%), while the horizontal axis indicates the evaluated methods. The size of each point is proportional to its corresponding training time, reflecting the computational cost. The results

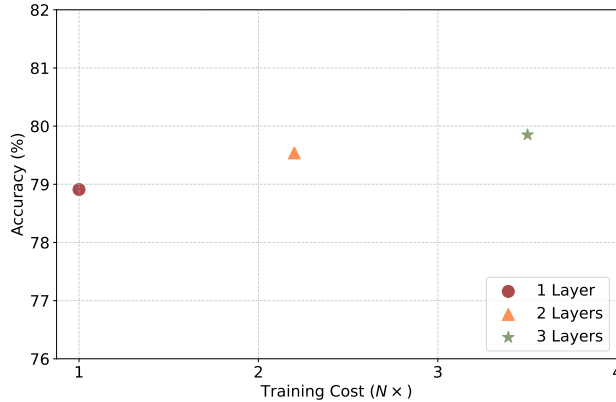


Figure 5: Impact of Posterior Modeling Depth on Accuracy and Training Cost.

demonstrate that BOGC achieves a desirable balance between accuracy and training overhead, delivering both strong performance and efficiency.

G.3 Posterior Modeling Depth

Our proposed method learns the posterior distribution over the parameters of the final layer in each modality-specific encoder. To further investigate the impact of posterior modeling depth on model performance and training cost, we conduct a comparative study by varying the number of layers included in the posterior modeling. Specifically, we evaluate three configurations where the posterior distribution is learned over the last one, two, or three layers of each encoder. All experiments are conducted on the CREMA-DOG dataset using a standard CNN-based architecture. As shown in Figure 5, model performance remains largely consistent across different modeling depths, whereas training cost increases exponentially with the number of layers involved in posterior modeling.